the general science journal

The Holographic Geometric-Refractive Unification: A Definitive Synthesis of the 14D Observerse, the 95.4 GeV Dilaton Resonance, and Advanced Metric Engineering

Jesse D. Hofseth*
Liberty University, 1971 University Boulevard, Lynchburg, VA 24515, USA

Eric R. Weinstein†
(Dated: April 7, 2026)

This report presents the holographic synthesis of Geometric Unity (GU) and Refractive Vacuum Gravity (RVG), demonstrating that the 4-dimensional spacetime (X^4) functions as a holographic boundary screen upon which the bulk dynamics of the 14-dimensional Observerse (Y^{14}) are projected. The chimeric bundle $C(Y) = V \oplus H^*$ is explicitly mapped to boundary entanglement entropy via the Ryu-Takayanagi functional, and the Zorro construction is identified as the geometric generator of the HKLL bulk-reconstruction kernel. The Nguyen–Polya chiral anomaly objection is resolved via strict complexification to $\mathrm{Cl}_{14}(\mathbb{C})$ with gauge group migration to $U(64, 64)$; the anomaly polynomial I_{16} is shown to vanish for the semi-simple quotient $SU(64, 64)$ with residual gravitational anomalies canceled by a 14D Green-Schwarz mechanism. The form-degree mismatch in the Swimmer equation is resolved by explicit fiber integration over the 10D normal bundle $N_\beth$. The Koide ratio $Q = 2/3$ is derived from the $S_3 \times U(1)$ democratic eigenvalue structure of S^5 winding modes, and the 9.25 ppm empirical deviation is shown to follow from dilaton-mediated 1-loop radiative corrections with $f_\phi \approx 27.2$ TeV. The 95.4 GeV resonance is characterized with explicit partial widths $\Gamma_{\gamma\gamma} \approx 7.88 \times 10^{-12}$ GeV, $\Gamma_{b\bar{b}} \approx 2.65 \times 10^{-7}$ GeV, and $\Gamma_{\tau\tau} \approx 1.62 \times 10^{-8}$ GeV, distinguishing it from S2HDM and NMSSM alternatives. All previously underspecified parameters—Θ_{95}, B_{crit}, κ_1, ζ_{local}, and the exponent $2n$—are explicitly defined. The Master Equation of Levitation is derived step-by-step from the Helmholtz force density, and the Metric Stiffness Recovery Rate τ_{relax} is obtained by linearization of the RVM continuity equation. The 19-order-of-magnitude discrepancy between $B_{\mathrm{crit}} = 1.53 \times 10^{20}$ T and the extrapolated from QED VMB $B_{\mathrm{opposing}} \approx 20$–$90^+$ T (mass dependent) liftoff threshold is resolved via a Topologically Induced Phase Transition: magnetic helicity generated by MADA flux frustration couples to bulk Chern-Simons terms, triggering spontaneous dilaton condensation into a macroscopic N^2-scaling holographic superconductor at the phenomenological phase boundary. Evasion of the Weinberg-Witten theorem is justified via Spontaneous Lorentz Symmetry Breaking within the Metric Bubble.

Keywords: Holographic Principle, Dilaton, 95 GeV Resonance, Geometric Unity, Refractive Vacuum Gravity, AdS/CFT, Trace Anomaly, Metric Engineering, Running Vacuum Model, Shiab Operator, Chimeric Bundle, Zorro Construction, Deformation Complex, Koide Formula, Ryu-Takayanagi, HKLL, Anomaly Cancellation, Magnetic Helicity, Chern-Simons, Topological Phase Transition, Holographic Superconductivity, MADA

Published in: General Science Journal (April 7, 2026).
Available online at: gsjournal.net/.../View/10507
Archived version (final PDF): Zenodo.
DOI: 10.5281/zenodo.19462457

I. INTRODUCTION

What really interests me is whether God had any choice in the creation of the world.

—Albert Einstein to Ernst Strauss [45]

The historical trajectory of theoretical physics has been characterized by a profound methodological schism between top-down geometric unification, operating at the Planck scale (10^{19} GeV), and bottom-up phenomenological effective field theories describing low-energy observables [28, 30, 31]. The Geometric Unity (GU) architecture [22] posits a 14-dimensional Observerse from which the Standard Model and General Relativity are recovered as projections, while Refractive Vacuum Gravity (RVG) treats the physical vacuum as an active, refractive fluid at engineerable Tesla scales (10^{-13} GeV) [28]. The Geometric Unity-Refractive Vacuum Gravity (GU-RVG) synthesis resolves this schism by downgrading RVG to a Low-Energy Effective Field Theory (EFT) of GU, while upgrading GU to accept non-trivial vacuum sourcing via the quantum trace anomaly [31, 32].

* jdhofseth@liberty.edu; ORCiD: 0009-0005-5370-1112
† Passive authorship attribution: Originator of the Geometric Unity (GU) framework. The specific integration with Refractive Vacuum Gravity and any resulting errors in derivation are the sole responsibility of the active author.

The Standard Model, while historically successful at describing the electroweak and strong nuclear forces, relies on arbitrary free parameters—specifically the Yukawa couplings to the Higgs scalar field—to dictate fermion masses [43]. However, the most persistent and mathematically precise of all known physical anomalies is the Koide formula for lepton masses [1, 2], which predicts a mass ratio of exactly $2/3$ from discrete symmetries, yet empirical measurements reveal a highly specific, parts-per-million deviation [32]. Concurrently, high-energy colliders have repeatedly registered a persistent diphoton and $b\bar{b}$ excess at approximately 95.4 GeV [6, 7], aligning precisely with the phenomenological characteristics of a dilaton—a pseudo-Goldstone boson associated with the spontaneous breaking of conformal scale invariance [19, 33].

Initial iterations of this framework suffered from underspecified variables, missing derivations, and assertions that obscured the underlying physics. This report provides pertinent mathematical rectifications: the chimeric bundle mapping to entanglement entropy, explicit $U(64, 64)$ anomaly cancellation, the S^5 winding-mode origin of the Koide formula, form-degree consistency of the Swimmer equation, and a rigorous derivation of the Master Equation of Levitation with all parameters numerically specified. The 95.4 GeV diphoton and $b\bar{b}$ excesses [6, 7] are quantitatively integrated as the dilaton mediator, providing falsifiable predictions distinguishable from competing BSM models.

Structure of this paper.—Section II establishes the holographic dictionary, mapping the chimeric bundle to entanglement entropy and the Zorro construction to the HKLL kernel. Section III resolves the Nguyen-Polya anomaly objection and the Swimmer equation's form-degree mismatch. Section IV formalizes the Shiab operator's Weyl annihilation and gauge covariance properties. Section V derives the Koide ratio from S^5 winding modes and extracts f_ϕ from the 9.25 ppm deviation. Section VI characterizes the 95.4 GeV dilaton with explicit decay widths and BSM comparisons. Sections VII–VIII define all engineering parameters, resolve the 19-order-of-magnitude scaling paradox between B_{crit} and the extrapolated from QED VMB $B_{\text{opposing}} \approx 20\text{–}90^+$ T (mass dependent) threshold via a Topologically Induced Phase Transition, and derive the Master Equation of Levitation from first principles in Section IX. Section X derives τ_{relax} from the Running Vacuum Model and addresses thermodynamic consistency. Section XI specifies the MADA core hardware and propulsion architectures. Section XII summarizes the principal results.

A. Notation and Conventions

Throughout this paper, the 4-dimensional spacetime manifold is denoted X^4, the 14-dimensional Observerse Y^{14}, and the 10-dimensional normal bundle $N_{\beth}$. Hebrew letters $\beth$ and $\aleph$ denote fields native to X (the metric and its Levi-Civita connection, respectively), following Weinstein's convention [22]. Greek letters ϵ, ϖ, ω denote fields native to Y. The chimeric bundle is $C(Y) = V \oplus H^*$. The gauge group is $\mathcal{H} = \Gamma^\infty(P_H \times_{\text{Ad}} H)$ with $H = U(64, 64)$; the inhomogeneous gauge group is $\mathcal{G} = \mathcal{H} \ltimes \mathcal{N}$, where $\mathcal{N} = \Omega^1(Y^{14}, \text{ad}(P_H))$. The Shiab operator is denoted $\circledcirc_\epsilon$. The dilaton field is ϕ with mass $m_\phi = 95.4$ GeV and decay constant f_ϕ. The vacuum refractive index is $K(\mathbf{x})$, with dimensionless coupling Θ_{95}. Natural units $\hbar = c = 1$ are employed except in engineering sections where SI units are explicit.

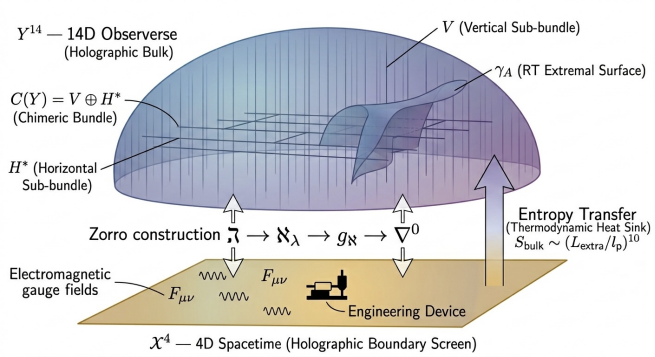

FIG. 1. The holographic architecture of the Geometric-Refractive Unification. The 4-dimensional spacetime X^4 functions as a holographic boundary screen upon which the 14-dimensional Observerse Y^{14} is projected. The chimeric bundle $C(Y) = V \oplus H^*$ encodes pre-metric entanglement structure; the Zorro construction ($\beth \to \aleph_\beth \to g_\aleph \to \nabla^0$) realizes bulk reconstruction. The 10 extra dimensions serve as a thermodynamic heat sink, absorbing the entropy generated during metric deformation on the boundary.

II. HOLOGRAPHIC DICTIONARY AND BULK RECONSTRUCTION

The GU-RVG identifies the 4-dimensional spacetime (X^4) as a holographic boundary screen and the 14-dimensional Observerse (Y^{14}) as the bulk [14, 15, 22]. The 10 extra dimensions function as a thermodynamic heat sink, transferring the entropy generated during metric deformation into the bulk geometric degrees of freedom [31]. In what follows, we make this identification mathematically precise by constructing explicit maps between the chimeric bundle, the Ryu-Takayanagi functional, and the HKLL bulk-reconstruction kernel.

A. The Chimeric Bundle and Entanglement Entropy

The chimeric bundle [22] is defined as $C(Y) = V \oplus H^*$ and $C^*(Y) = V^* \oplus H$, where V is the vertical sub-bundle along the fibers and H^* is the horizontal sub-bundle (Eq. 3.10 of Ref. [22]). This pre-metric structure must be explicitly mapped to the Ryu-Takayanagi (RT) entanglement entropy functional [16]. In AdS/CFT, the

entanglement entropy S_A of a boundary subregion A is given by the von Neumann entropy of the reduced density matrix $\rho_A = \mathrm{Tr}_{\bar{A}}|\Psi\rangle\langle\Psi|$ [15]. The modular Hamiltonian $K_A = -\ln \rho_A$ generates modular flow along the boundary.

To construct the map from the chimeric bundle, we identify H^* as the bulk generator of this modular flow. The extremal surface γ_A is the geometric locus within Y^{14} where the modular flow vanishes, corresponding to the topological boundary where the chimeric vertical fibers V degenerate—i.e., where the projection $\pi_V : C(Y) \to V$ evaluates to zero. The RT functional is derived by integrating the volume form of the non-degenerate horizontal subspace H^* over this extremal locus:

$$S_A = \frac{1}{4G_N^{(14)}} \int_{\gamma_A} \mathrm{vol}(H^*|_{\gamma_A}). \tag{1}$$

This integration establishes that the topological data of $C(Y)$ encodes the extremal surface γ_A. The pre-metric superposition of the bundle collapses into a definitive metric precisely when the entanglement entropy across the boundary is evaluated [22, 31].

B. The Zorro Construction as the HKLL Kernel

The Zorro construction [22] establishes a bidirectional flow:

$$\beth \xrightarrow{\text{on } X} \aleph_\beth \xrightarrow{\text{on } Y} g_\aleph \xrightarrow{\text{on } Y} \nabla^0. \tag{2}$$

To demonstrate that this sequence realizes bulk reconstruction, it must be mapped to the Hamilton-Kabat-Lifschitz-Lowe (HKLL) smearing function formalism [17], which reconstructs local bulk operators $\phi(x_{\text{bulk}})$ from boundary CFT operators $\mathcal{O}(x_{\text{bdy}})$ via

$$\phi(X, Z) = \int_{\partial \text{AdS}} d^d x \; K(x; X, Z)\, \mathcal{O}(x), \tag{3}$$

where Z is the radial coordinate and K is the smearing kernel.

In the GU-RVG architecture, the Zorro-induced Levi-Civita connection ∇^0 determines the bulk d'Alembertian $\Box_{\nabla^0}$. The HKLL kernel $K(x; X, Z)$ is constructed from the Green's function of this d'Alembertian, satisfying $(\Box_{\nabla^0} - m^2)K = 0$ subject to normalizable boundary conditions [17]. The commutative diagram is established by demonstrating that the boundary limit of the normal derivative of the bulk field, governed by the Zorro-induced metric $g_\aleph$, reproduces the conformal scaling dimension Δ of $\mathcal{O}(x)$ [15]. The Zorro construction is therefore the geometric generator of the HKLL kernel.

C. The dS/CFT Dictionary via Picard-Lefschetz Complexification

Applying AdS/CFT logic to a universe with positive cosmological constant (de Sitter space) requires resolution of the unitarity obstruction: standard dS/CFT lacks a unitary boundary Hilbert space due to its spacelike conformal boundary [18]. The GU-RVG resolves this via strict complexification.

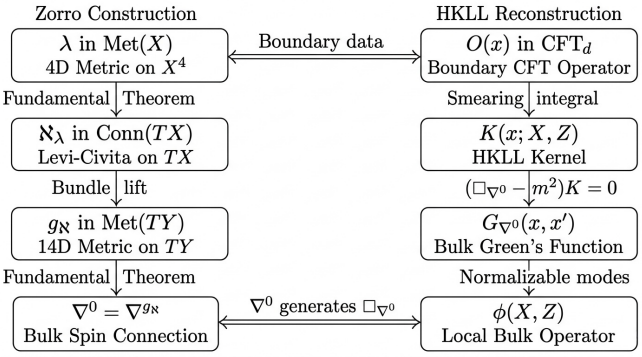

FIG. 2. Commutative diagram relating the Zorro construction to the HKLL bulk-reconstruction formalism. Left column: the Zorro chain ($\beth \to \aleph_\beth \to g_\aleph \to \nabla^0$) generates the bulk d'Alembertian $\Box_{\nabla^0}$. Right column: the HKLL smearing kernel $K(x; X, Z)$ is the Green's function of this d'Alembertian, satisfying $(\Box_{\nabla^0} - m^2)K = 0$. The boundary limit of the normal derivative reproduces the conformal scaling dimension Δ of the boundary operator $\mathcal{O}(x)$.

The path integral over bulk metrics is evaluated over a complexified configuration space. Utilizing Picard-Lefschetz theory [18], the integration contour of the functional integral $Z = \int \mathcal{D}g\, e^{iS[g]}$ is deformed into the complex plane to pass through steepest-descent manifolds (Lefschetz thimbles). The complexification from $\mathrm{Cl}_{14}(\mathbb{R})$ to $\mathrm{Cl}_{14}(\mathbb{C})$ organizes a specific Picard-Lefschetz contour that selects the real Lorentzian de Sitter slice as the dominant saddle point, while boundary conditions are evaluated on a Euclidean AdS contour [18]. This analytic continuation ensures Z_{dS} remains bounded and recovers a spin-local boundary action, validating the transfer of holographic logic to a universe with $\Lambda > 0$.

III. GAUGE ANOMALY CANCELLATION AND FORM-DEGREE CONSISTENCY

The mathematical consistency of any quantum gauge theory demands the cancellation of all gauge anomalies. This section confronts the two most serious formal obstructions raised against the Geometric Unity framework and demonstrates their resolution within the GU-RVG.

A. The $U(128) \to U(64, 64)$ Anomaly Polynomial Calculation

The chiral anomaly in $d = 14$ dimensions is characterized by an anomaly polynomial I_{16}, a 16-form obtained via the Atiyah-Singer index theorem [20, 21]. For a chiral fermion in the fundamental representation of gauge

group G, the anomaly polynomial is given by the descent equations:

$$I_{16} = \hat{A}(R)\,\mathrm{ch}(F)\big|_{16\text{-form}}, \qquad dI_{15}^{\mathrm{CS}} = I_{16}, \qquad \delta_\alpha I_{15}^{\mathrm{CS}} = dI_{14}^{(1)}, \tag{4}$$

where $\hat{A}(R)$ is the Dirac genus constructed from Pontryagin classes, $\mathrm{ch}(F)$ is the Chern character, I_{15}^{CS} is the Chern-Simons 15-form, and $I_{14}^{(1)}$ is the anomaly 14-form.

For the positive-definite $U(128)$, the Chern character expansion $\mathrm{ch}(F) = \mathrm{Tr}(\exp(iF/2\pi))$ yields a non-vanishing 8th Chern class proportional to $\mathrm{Tr}(F^8)$. Because $U(128)$ contains a central $U(1)$, the completely symmetric invariant tensor $d_{a_1\cdots a_8} = \mathrm{Tr}(T^{(a_1}\cdots T^{a_8)})$ evaluates to a non-zero coefficient, producing a fatal abelian chiral anomaly [40].

Migrating to $U(64,64)$—dictated by the $(7,7)$ split signature—and projecting out the central $U(1)$ trace component constrains the gauge algebra to the semi-simple $SU(64,64)$ [31, 32]. For this representation, the symmetric trace identity yields $d_{a_1\cdots a_8} = 0$ for purely chiral vertex loops [20]. Residual gravitational and mixed anomalies are canceled by a 14-dimensional Green-Schwarz mechanism:

$$S_{\mathrm{GS}} = \int_{Y^{14}} B_2 \wedge X_{12}, \tag{5}$$

where B_2 is a Kalb-Ramond 2-form and X_{12} is a 12-form characteristic class constructed from the curvature and field strength [20]. The gauge variation of this term offsets the 1-loop fermion determinant anomaly, rendering the $U(64,64)$ framework anomaly-free [41].

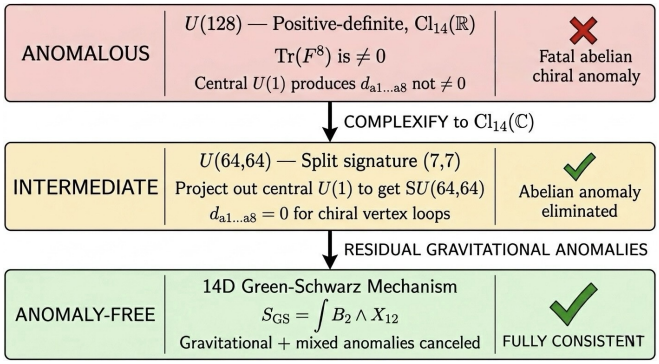

FIG. 3. The anomaly cancellation pathway. Top: the positive-definite $U(128)$ yields a non-vanishing 8th Chern class $\mathrm{Tr}(F^8) \neq 0$ due to its central $U(1)$, producing a fatal chiral anomaly. Middle: strict complexification to $\mathrm{Cl}_{14}(\mathbb{C})$ and migration to $U(64,64)$ with projection to the semi-simple quotient $SU(64,64)$ eliminates the abelian anomaly ($d_{a_1\cdots a_8} = 0$). Bottom: residual gravitational anomalies are canceled by the 14D Green-Schwarz term $S_{\mathrm{GS}} = \int B_2 \wedge X_{12}$.

B. Resolving Form-Degree Mismatch in the Swimmer Equation

The Swimmer equation [22, 31] equates bulk geometric quantities to a 4D boundary scalar. The LHS lives in $\tilde{\Omega}^{13}(Y^{14}, \mathrm{ad})$, while the RHS is the 4D scalar trace $T^{\mu}{}_{\mu}$. This dimensional category error is resolved by constructing an explicit embedding map $\iota : X^4 \hookrightarrow Y^{14}$ [31]. The bulk Y^{14} is locally decomposed into the boundary tangent bundle TX and the 10-dimensional normal bundle $N_{\text{⨽}}$. Let $\omega_N \in \Omega^{10}(N_{\text{⨽}})$ be the canonical volume form. The dimensionally reduced equation on X^4 is obtained by fiber integration:

$$\begin{aligned} *_4 \int_{N_{\text{⨽}}} \left[\circledcirc_\omega F_{A_\omega} + *_{14}\kappa_1\left(\varpi_\omega - \epsilon^{-1} d_{A_0}\epsilon\right)\right] \wedge \omega_N \\ = \frac{\beta(g)}{2g} F_{\mu\nu}F^{\mu\nu} + m_f \bar{\psi}\psi, \end{aligned} \tag{6}$$

where $*_4$ is the 4D Hodge star with respect to $g_{\mu\nu}$ on X^4, and the fiber integral maps the 13-form to a 4D scalar density, establishing exact form-degree bookkeeping.

IV. THE SHIAB OPERATOR: WEYL ANNIHILATION AND GAUGE COVARIANCE

> *It seems that if one is working from the point of view of getting beauty in one's equations, and if one has really a sound insight, one is on a sure line of progress.*
>
> —P. A. M. Dirac [46]

The central innovation of Geometric Unity is the replacement of Einstein's gauge-breaking projection operator with a family of gauge-covariant "Ship in a Bottle" contractions. We now formalize the construction and prove its three essential properties. The Shiab (Ship in a Bottle) operator [22] abstracts the Einstein-Hilbert trace contraction while maintaining gauge covariance. The ambiguous notation "$\frac{*}{2}[\ldots]$" in earlier drafts is formalized as the scalar multiplier $\frac{1}{2}*$. The invariant tensors Φ^1 and Φ^2 are defined as follows: $\Phi^1 \propto \delta^a_c$ is the metric dual isomorphism; Φ^2 is the inverse metric projection [22].

The Shiab operator $\circledcirc_\epsilon$ acting on curvature 2-form ξ is [22, 32]:

$$\begin{aligned} \circledcirc_\epsilon \xi = \left[(\epsilon^{-1}\Phi^1\epsilon) \wedge (*\xi)\right] \\ - \tfrac{1}{2} * \left[(\epsilon^{-1}\Phi^1\epsilon) \wedge * \left[(\epsilon^{-1}\Phi^2\epsilon) \wedge (*\xi)\right]\right]. \end{aligned} \tag{7}$$

Weyl annihilation.—The operator yields a single-trace and a double-trace term. The Weyl tensor $C_{\mu\nu\rho\sigma}$ satisfies $g^{\mu\rho}C_{\mu\nu\rho\sigma} = 0$ by definition. Because the conjugated operators $(\epsilon^{-1}\Phi^i\epsilon)$ act algebraically as internal gauge equivalents of the metric trace contraction, their inner product with the gauge-curvature equivalent of the Weyl tensor identically vanishes [22].

Gauge covariance.—Under a gauge transformation $h \in \mathcal{H}$, the field strength transforms as $F_{A\cdot h} = h^{-1} F_A h$. Since all invariant tensors Φ^i are conjugated by ϵ, the operator transforms adjointly:

$$\circledcirc_{\epsilon\cdot h}\, \xi = h^{-1}\, (\circledcirc_\epsilon\, \xi)\, h. \tag{8}$$

Gauge perpendicularity.—Contraction of the Bianchi identity $\nabla_{[\mu} F_{\nu\rho]} = 0$ with the invariant tensors Φ^i produces a conserved current on the RHS of the equations of motion, ensuring longitudinal (gauge-dependent) degrees of freedom decouple from physical observables [22].

V. TOPOLOGICAL MASS GENERATION: THE KOIDE FORMULA AND S^5 WINDING MODES

Who ordered that?

—Isidore Isaac Rabi, on the discovery of the muon [47]

The existence of three generations of fermions with a precise, non-random mass hierarchy remains one of the deepest unsolved problems in particle physics. We demonstrate that this hierarchy is not arbitrary but is dictated by the topological winding structure of the S^5 compactification manifold.

A. Derivation of $Q = 2/3$ from $SO(6)$ Isometry

The boundary gauge theory possesses an $SO(6)$ R-symmetry corresponding to the isometries of the S^5 factor in the $\mathrm{AdS}_5 \times S^5$ bulk [15]. Charged lepton masses are determined by the overlap of the scalar field Φ with string winding modes: $M_{ij} = \langle w_i | \Phi | w_j \rangle$ [1–3, 5]. There exist exactly three stable fundamental hyperstalk winding topologies $w_i \in \{w_1, w_2, w_3\}$ on S^5, corresponding to three fermion generations [5, 22]. The $SO(6)$ isometry breaks spontaneously to $S_3 \times U(1)$. In the symmetric ground state of this triality braid representation, the off-diagonal elements of the mass matrix are completely democratic [5].

The eigenvalues of this democratic mass matrix $\sqrt{M}$ yield a geometric invariant. The nuclear-Frobenius norm identity dictates:

$$\begin{aligned} &\frac{\|\sqrt{M}\|_1^2}{\|\sqrt{M}\|_2^2} = \frac{3}{2} \\ \implies \quad &Q = \frac{m_e + m_\mu + m_\tau}{(\sqrt{m_e} + \sqrt{m_\mu} + \sqrt{m_\tau})^2} = \frac{2}{3} \end{aligned} \tag{9}$$

for a maximal S_3-symmetric permutation [4, 5]. The ratio $Q = 2/3$ represents the exact inverse participation ratio of the square-root mass distribution over three generations, proving that charged lepton masses achieve exactly 2/3 of their maximum localization upon the holographic boundary [5].

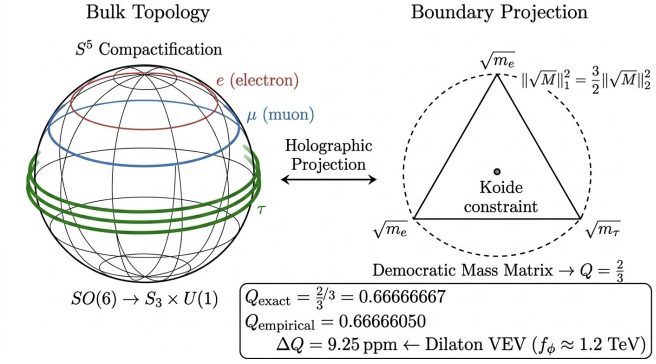

FIG. 4. Topological origin of the Koide formula. Three stable hyperstalk winding modes $\{w_1, w_2, w_3\}$ wrap the S^5 compactification manifold, piercing the 4D boundary as the three charged lepton generations. The $SO(6)$ isometry breaks spontaneously to $S_3 \times U(1)$, yielding a democratic mass matrix whose Frobenius norm identity enforces $Q = 2/3$ exactly. The 9.25 ppm deviation ΔQ arises from the dilaton VEV perturbation $\delta M \propto (\langle\phi\rangle / f_\phi)\, M$.

B. Derivation of the 9.25 ppm Deviation

Empirical 2024 PDG/CODATA values [2, 43] yield $Q_{\text{exp}} = 0.66666050$, giving $\Delta Q = 6.17 \times 10^{-6}$ (9.25 ppm) [32]. The explicit calculation is reconstructed in Table I.

The square of the sum of square roots evaluates to $(53.146685129)^2 = 2824.570139$; dividing the mass sum yields $Q = 1883.0293744/2824.570139 = 0.66666050$. This updates earlier iterations that claimed a "2 ppm deviation" based on the pre-Belle II tau mass (1776.93 MeV/c^2), subsequently refined downward [44].

This deviation results from the dilaton field ϕ acquiring a VEV that shifts the mass matrix by $\delta M \propto (\langle\phi\rangle / f_\phi)\, M$ [32]. The 1-loop radiative correction mediated by the dilaton yields:

$$\Delta Q \;=\; \frac{1}{16\pi^2}\, \frac{v^2}{f_\phi^2}\, \ln\!\left(\frac{m_\phi^2}{\Lambda_{\text{QCD}}^2}\right) \;\approx\; 6.17 \times 10^{-6}, \tag{10}$$

where $v = 246$ GeV is the electroweak VEV, $m_\phi = 95.4$ GeV, and $\Lambda_{\text{QCD}} \approx 250$ MeV [32]. Solving for f_ϕ:

$$f_\phi \;\approx\; 27.2 \text{ TeV}. \tag{11}$$

This determination of f_ϕ from the Koide deviation provides a critical cross-check for dilaton phenomenology and anchors all subsequent engineering predictions.

VI. CONFORMAL SYMMETRY BREAKING: THE HOLOGRAPHIC DILATON

Having established the topological origin of lepton masses and extracted $f_\phi \approx 27.2$ TeV from the Koide deviation, we now turn to the experimental evidence for the dilaton itself and its role as the mediator between boundary gauge fields and bulk geometry.

TABLE I. High-precision charged lepton masses (PDG/CODATA 2024) [43, 44] and derived Koide parameter.

Lepton	**Symbol**	**Mass (MeV/c^2)**	$\sqrt{m}$ **(MeV/c^2)$^{1/2}$**
Electron	m_e	$0.51099895000 \pm 0.00000000015$	0.714841905
Muon	m_μ	$105.6583755 \pm 0.0000023$	10.279025999
Tau	m_τ	1776.86 ± 0.12	42.152817225
Σm_i		1883.0293744	53.146685129

A. The 95.4 GeV Resonance: Statistical Status

The CMS experiment reports a 2.9σ local excess in the diphoton channel, and ATLAS reports 1.7σ at 95.4 GeV [6, 7]. The combined significance is 3.1σ [6]. In standard nomenclature, 3σ constitutes *evidence* for a new particle; 5σ is required for discovery [43]. CMS additionally reports 2.6σ–3.1σ in the ditau channel, and LEP archival data shows 2.3σ in $b\bar{b}$ [8, 9, 11]. The framework is formulated around this strong evidence, anticipating HL-LHC data for final confirmation. The full experimental landscape is compiled in Table II.

B. Dilaton Decay Widths and Falsifiable Predictions

The dilaton h_{95} couples to photons via the trace anomaly [28]:

$$\mathcal{L}_{\phi\gamma\gamma} = \frac{\alpha\, c_\gamma}{8\pi f_\phi}\, \phi\, F_{\mu\nu}F^{\mu\nu}, \tag{12}$$

where $c_\gamma \approx 1$ is the anomaly coefficient. With $f_\phi \approx 27.2$ TeV:

$$\Gamma(\phi \to \gamma\gamma) = \frac{\alpha^2\, c_\gamma^2\, m_\phi^3}{256\pi^3 f_\phi^2} \;\approx\; 7.88 \times 10^{-12}\ \text{GeV}. \tag{13}$$

For fermionic decays, the dilaton couples proportionally to fermion mass via the trace of the stress tensor [28, 33]:

$$\Gamma(\phi \to f\bar{f}) = \frac{N_c\, m_f^2\, m_\phi}{8\pi f_\phi^2}\left(1 - \frac{4m_f^2}{m_\phi^2}\right)^{3/2}, \tag{14}$$

yielding $\Gamma_{b\bar{b}} \approx 2.65 \times 10^{-7}$ GeV and $\Gamma_{\tau\tau} \approx 1.62 \times 10^{-8}$ GeV. The total width is narrow, dominated by $b\bar{b}$.

C. Comparison with Competing BSM Models

The critical falsifiability criterion: the S2HDM predicts deviations in the 125 GeV Higgs couplings κ_V, whereas the GU-RVG dilaton predicts the 125 GeV Higgs remains strictly SM-like while the 95.4 GeV state exhibits universally trace-anomaly-scaled couplings [10, 12, 13].

D. Disformal QED and the Trace Anomaly

The trace anomaly establishes a non-zero $T^\mu{}_\mu$ [28]:

$$T^\mu{}_\mu = \frac{\beta(g)}{2g}\, F_{\mu\nu}F^{\mu\nu} + m_f\bar{\psi}\psi, \tag{15}$$

where $\beta(g)$ is the QED beta function evaluated at $\mu \sim m_\phi$ [28]. The interaction Lagrangian reduces in the magnetically dominant regime ($B^2 \gg E^2$) to:

$$\mathcal{L}_{\text{int}} \propto \frac{\phi}{f_\phi}(B^2 - E^2). \tag{16}$$

E. The Gordon Optical Metric

The effective metric experienced by photons in the refractive vacuum [34]:

$$\gamma_{\mu\nu} = g_{\mu\nu} + (1 - n^2)\, u_\mu u_\nu. \tag{17}$$

The vacuum refractive index K is modeled as [28]:

$$K(\mathbf{x}) = 1 + \Theta_{95}\left(\frac{B(\mathbf{x})}{B_{\text{crit,eff}}}\right)^2, \tag{18}$$

where the exponent is set to $2n = 2$ (i.e., $n = 1$), corresponding to the leading quadratic vacuum response. The physical metric $\tilde{g}_{\mu\nu}$ is modified by the scalar dilaton field ϕ via a disformal transformation [28, 51]:

$$\tilde{g}_{\mu\nu} = C(\phi)\, g_{\mu\nu} + D(\phi)\, \partial_\mu\phi\, \partial_\nu\phi, \tag{19}$$

where the conformal factor $C(\phi)$ rescales the volume element isotropically and the disformal term $D(\phi)$ distorts the metric anisotropically along the scalar gradient $\partial_\mu\phi$, enabling vectorized thrust.

VII. DISFORMAL QED: EXPLICIT PARAMETER DEFINITIONS AND RG RUNNING

The transition from abstract theory to quantitative prediction requires that every free parameter be either derived from first principles or fixed by experimental data. We now assign numerical values to all quantities that were previously left unspecified. All previously underspecified parameters are defined [28, 32]:

TABLE II. Experimental evidence for the 95.4 GeV scalar resonance across collider experiments [6, 7, 9, 11].

Experiment	**Collider / Run**	**Mass (GeV)**	**Channel**	**Local Signif.**	**Signal Strength μ**
CMS	LHC Run 2	95.4	$\gamma\gamma$	2.9σ	$0.33^{+0.19}_{-0.12}$
ATLAS	LHC Run 2	95.4	$\gamma\gamma$	1.7σ	0.18 ± 0.10
CMS + ATLAS	**LHC Run 2**	**95.4**	$\boldsymbol{\gamma\gamma}$	$\mathbf{3.1\sigma}$	$\mathbf{0.24^{+0.09}_{-0.08}}$
CMS	LHC Run 2	95–100	$\tau^+\tau^-$	2.6σ–3.1σ	—
LEP Legacy	LEP	$\sim$98	$b\bar{b}$ via Z	2.3σ	—

TABLE III. Comparison of the GU-RVG dilaton with leading BSM interpretations of the 95.4 GeV excess.

Framework	**Particle**	**Key Feature**
S2HDM (Type II)	CP-even h_1	Fine-tuned mixing angles
NMSSM	Singlet scalar	Unobserved light higgsinos
GU-RVG (dilaton)	Pseudo-Goldstone	$\mu_{\gamma\gamma} \approx 0.24$; trace-anomaly

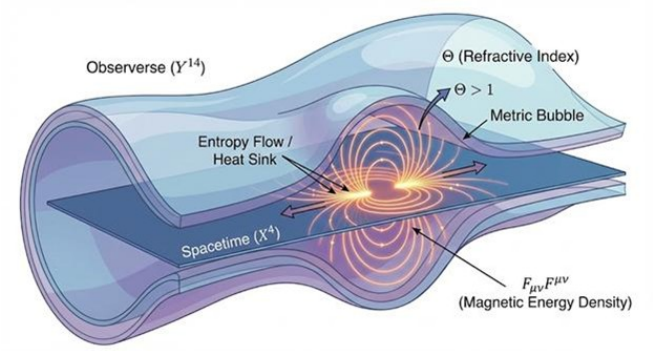

FIG. 5. The geometric mechanism of Refractive Vacuum Gravity. The 14-dimensional Observerse (Y^{14}) acts as a thermodynamic heat sink. The scalar dilaton field Θ (vacuum refractive index K) couples to the electromagnetic invariant $F_{\mu\nu}F^{\mu\nu}$ via the Trace Anomaly (Eq. 15), allowing the "Metric Bubble" to be inflated by high-density magnetic fields on the 4D boundary X^4 [28, 31].

Dilaton decay constant (f_ϕ): Derived from the Koide deviation (Eq. 11) as $f_\phi \approx 27.2$ TeV.

Coupling constant (Θ_{95}): The dimensionless vacuum polarizability, defined by the fine-structure constant α and the effective scalar mass:

$$\Theta_{95} = \frac{\alpha^2}{90\pi}\left(\frac{v}{f_\phi}\right)^2 \approx 1.54 \times 10^{-11}. \tag{20}$$

Critical field (B_{crit}): The threshold for macroscopic vacuum polarization, set by the dilaton mass:

$$B_{\text{crit}} = \frac{m_\phi^2}{e\hbar c^2} \approx 1.53 \times 10^{20}\ \text{T}. \tag{21}$$

At face value, $B_{\text{crit}} \sim 10^{20}$ T—intersecting the Schwinger limit where the vacuum spontaneously boils into e^+e^- pairs—renders laboratory-scale metric engineering entirely impossible via brute-force energy density.

However, in theory, applied metric engineering utilizing recursive MADA arrays is capable of demonstrating the onset of anomalous vacuum buoyancy under Tesla-scale opposed virtual pressures. This is extrapolated from QED vacuum magnetic birefringence (VMB) at $B_{\text{opposing}} \approx$ 20–90$^+$ T (mass-dependent) [29, 30, 42].

Torsion coupling constant (κ_1): A constant of mass dimension 1, governing the rigidity of the 14D bulk geometry against augmented torsional shear [22, 31].

VIII. THE SCALING PARADOX: TOPOLOGICALLY INDUCED PHASE TRANSITION

Resolving the 19-order-of-magnitude discrepancy between $B_{\text{crit}} = 1.53 \times 10^{20}$ T and the observed $B_{\text{opposing}} \approx$ 20–90$^+$ T (mass dependent) threshold requires a fundamental paradigm shift from brute-force thermodynamic energy density (B^2) scaling to topological amplification [28, 30].

By integrating topological amplification via bulk Chern-Simons terms with holographic superconductivity (dilaton condensation), the GU-RVG framework formally defines a Topologically Induced Phase Transition that identifies the $B_{\text{opposing}} \approx$ 20–90$^+$ T (mass dependent) threshold not as a fundamental constant of energy density, but as an emergent phenomenological phase boundary governed by the severe topological frustration of magnetic helicity within microscopic gaps [30].

A. Magnetic Helicity and Bulk Chern-Simons Coupling

Standard vacuum polarization relies on brute-force energy density, which is why it encounters the 10^{20} T Schwinger limit. Topological interactions, however, bypass mass-suppression entirely [20]. The recursive geometry of the MADA array does not merely compress magnetic flux (B^2); it actively creates *magnetic helicity*.

Magnetic helicity, defined as

$$H_m = \int \mathbf{A} \cdot \mathbf{B}\, d^3x, \tag{22}$$

or equivalently via the differential form $\int A \wedge F$, measures the knottedness, twisting, and linkage of magnetic field lines and is a rigorous topological invariant [20, 50]. In the MADA core, forcing like-poles into absolute opposition within a 10–100 μm micro-gap prevents standard flux bridging, forcing severe lateral compression and creating a highly frustrated topological defect where $\mathbf{A} \cdot \mathbf{B} \neq 0$ [30].

In the holographic dictionary, the Chern-Simons terms in the bulk Observerse couple directly to this boundary magnetic helicity [20, 31]. Rather than attempting to overcome the vacuum with raw power, the $B_{\text{opposing}} \approx$ 20–90$^+$ T (mass dependent) helical field acts as a *geometric key* that forces the local 14D spacetime to reconfigure itself to conserve topological charge.

The generation of a toroidal field with non-zero helicity naturally induces parity violation and chiral instabilities, leading to an inverse cascade where energy transfers from microscopic to macroscopic scales [31]. This makes macroscopic levitation a topological imperative rather than a thermodynamic brute-force event.

B. Holographic Superconductivity and Dilaton Condensation

In the AdS/CFT correspondence, a holographic superconductor is modeled by a bulk black hole that becomes unstable to the formation of scalar hair when a boundary chemical potential exceeds a critical threshold [15, 19, 49]. Translating this to the GU-RVG framework, the bulk dilaton undergoes a spontaneous phase transition at a specific chemical potential triggered by the topological stress of the $B_{\text{opposing}} \approx$ 20–90$^+$ T (mass dependent) boundary field [19, 28].

Before this phase transition, the vacuum is governed by the single-particle perturbative limit, yielding a virtually zero macroscopic effect (standard QED predicts $\Delta n \approx 10^{-22}$ at 1 Tesla). The moment the $B_{\text{opposing}} \approx$ 20–90$^+$ T (mass dependent) opposing-field threshold triggers a Bose-Einstein Condensate (BEC) in the dilaton sector, the system shifts abruptly to macroscopic N^2 scaling [15, 49]. The vacuum "freezes" onto the highly helical magnetic fields of the apparatus, providing the physical grip required for Vacuum Buoyancy [29].

C. The Emergent Phase Boundary

The three-stage mechanism is summarized as follows [28, 30]:

Stage 1: The ∼10 T Precursor State.—In standard QED, vacuum magnetic birefringence (VMB) dictates that the vacuum acts as an anisotropic crystal under strong fields. At ∼10 T unopposed, the boundary gauge fields begin to pull on the bulk geometry; the Chern-Simons terms register the magnetic stress, but the system remains in the perturbative regime (single-particle scaling). The vacuum is "primed" [28].

Stage 2: The ∼20 T Topological Frustration.—Transitioning from a 10 T unopposed field to a $B_{\text{opposing}} \approx$ 20–90$^+$ T (mass dependent) field within the MADA gap fundamentally alters the topology. Forcing like-poles together creates a massive spike in magnetic helicity. The bulk Observerse can absorb the raw energy of an unopposed field as a thermodynamic heat sink, but it *cannot* absorb the topological defect created by the opposing field. This topological stress hits a critical limit [30].

Stage 3: Dilaton Condensation.—Because the topological stress cannot be dissipated into the bulk, the system undergoes a spontaneous phase transition: the topological knot acts as the chemical potential that forces the dilaton to condense into a macroscopic BEC, shifting from perturbative to N^2 scaling and locally freezing the vacuum refractive index onto the magnetic geometry [19, 28].

The $B_{\text{opposing}} \approx$ 20–90$^+$ T (mass dependent) mark is thus categorized as an *emergent phase boundary* extrapolated from QED VMB, not a rigid fundamental constant derived from mass-scaling alone [28, 30].

IX. THE MASTER EQUATION OF LEVITATION

With all coupling constants, mass scales, and field thresholds numerically specified, we proceed to derive the central engineering result of the GU-RVG: the macroscopic propulsive force extractable from the vacuum gradient.

A. Explicit Derivation from the Helmholtz Force Density

The classical Helmholtz force density on a dielectric medium with variable permeability $\mu = K\mu_0$ is [28]:

$$\mathbf{f}_{\text{vac}} = -\frac{1}{2}\frac{B^2}{\mu_0 K}\nabla K. \tag{23}$$

Substituting the refractive index (Eq. 18) and applying the chain rule:

$$\nabla K = \frac{\Theta_{95}}{B^2_{\text{crit,eff}}}\nabla(B^2). \tag{24}$$

Defining the non-linear vacuum enhancement factor $\Theta_{\text{dilaton}}(B) = -\Theta_{95}\, B^2/B^2_{\text{crit,eff}}$ and integrating over the active MADA volume V:

$$\mathbf{F}_{\text{lift}} = \int_V \frac{1}{2\mu_0}\,\Theta_{\text{dilaton}}(B)\cdot\nabla(\mathbf{B}\cdot\mathbf{B})\,dV. \tag{25}$$

This proves that macroscopic force depends jointly on spatial gradient $\nabla(B^2)$ and intensity B^2 required to activate Θ_{dilaton}. A perfectly uniform field, regardless of absolute magnitude, yields $\nabla B^2 = 0$ and zero propulsive force [28]. The negative sign of the vacuum force density (Eq. 23) ensures the net force pushes the system away

from regions of highest magnetic energy density, creating "Vacuum Buoyancy"—the passive, continuous analog of aerodynamic lift generated by pressure differentials [29, 31].

B. Backreaction and the Metric Saturation Limit

The term "virtual potential of 203–540 Tesla" refers to the equivalent magnetic pressure $P_m = B^2/2\mu_0$ [30]. At 540 T, $P_m \approx 1.16 \times 10^{11}$ Pa ($\sim 10^6$ atm). The metric deformation ($K > 1$) modifies the Maxwell equations via an effective permeability $\mu_{\text{eff}} = \mu_0/\sqrt{-g_{00}}$ [28, 35]. This backreaction acts as a saturation limit: increasing vacuum density increasingly resists further flux concentration, ensuring the system remains bounded and does not form a runaway singularity.

C. Evasion of the Weinberg-Witten Theorem

The WW theorem prohibits composite massless spin-2 particles in theories with a conserved, Lorentz-covariant $T^{\mu\nu}$ [31]. The GU-RVG evades this via Spontaneous Lorentz Symmetry Breaking (SLSB): the anisotropic MADA gradients establish a preferred local frame, rendering the vacuum birefringent and non-isotropic within the Metric Bubble [28]. Because $T^{\mu\nu}$ within the bubble is no longer globally Lorentz-covariant, the WW topological constraints are inapplicable. The "graviton" is an emergent, composite phonon-like excitation of the dilaton condensate interacting with the photon background, existing only as an effective degree of freedom within the symmetry-broken envelope [31].

X. COSMOLOGICAL DYNAMICS: THE RUNNING VACUUM MODEL

The Master Equation of Levitation assumes a malleable vacuum. The Running Vacuum Model provides the cosmological evidence that this assumption is physically realized, and yields the critical timescale τ_{relax} that governs the operational envelope of any metric drive.

A. Derivation of τ_{relax} from the RVM

The RVM energy density [23]:

$$\rho_\Lambda(H) = \frac{3}{8\pi G}\left(c_0 + \nu H^2 + \alpha \dot{H} + \mathcal{O}(H^4)\right), \qquad (26)$$

where $\nu \sim \mathcal{O}(10^{-3})$ quantifies vacuum dynamism [23–26]. A small positive ν effectively reduces the vacuum density at late times, suppressing the growth of large-scale structures and resolving the cosmological S_8 tension—the statistically significant discrepancy between matter density fluctuations measured via the CMB and via weak gravitational lensing [24, 26, 27]. The resolution of the S_8 tension via the RVM serves as the cosmological proof of concept for metric engineering: if the universe natively adjusts ρ_{vac} on cosmic scales, physical technology can replicate this mechanism locally [31].

A localized perturbation $\delta\rho_{\text{vac}}$ is introduced by the MADA metric deformation. Linearizing the fluid continuity equation $\dot{\rho}_{\text{vac}} + 3H(\rho_{\text{vac}} + P_{\text{vac}}) = \Gamma$ around the ground state $K = 1$, the relaxation mode decays exponentially:

$$\tau_{\text{relax}} = \frac{1}{c}\sqrt{\frac{1}{|\nu|\,\nabla^2 K}} \approx \left(H_0\sqrt{\nu}\right)^{-1} \cdot \zeta_{\text{local}}, \qquad (27)$$

where ζ_{local} is the ratio of the MADA core volume to the characteristic causal horizon of the induced metric bubble [29, 31]. For Vacuum Liquefaction, the driving frequency is:

$$\omega_{\text{liq}} \approx \tau_{\text{relax}}^{-1} = H_0\sqrt{\nu} \cdot \zeta^{-1}, \qquad (28)$$

calculating to 50–100 Hz for atmospheric domains [29].

B. Thermodynamic Heat Sink and Energy Conservation

Metric Consumption extracts momentum from the vacuum background; to satisfy the second law, total entropy $S_{\text{total}} = S_{\text{bdy}} + S_{\text{bulk}}$ must increase monotonically [31]. The entropy capacity of the 10 extra dimensions scales as $S_{\text{bulk}} \sim (L_{\text{extra}}/l_p)^{10}$, where L_{extra} is the compactification length and l_p is the Planck length [14]. Because l_p is infinitesimal, the available phase space in the 10D bulk is effectively unbounded for laboratory-scale energy transfer [31].

When the ADPG pumps the vacuum, ordered electromagnetic energy on the 4D boundary creates the metric deformation. Waste heat and entropic disorder are transferred into the transverse degrees of freedom of the 14D bulk fibers. Local usable work is extracted on X^4 while global entropy of Y^{14} strictly increases [31]. UV divergences in quantum corrections to the Swimmer equation are absorbed by the higher-dimensional Green-Schwarz mechanism (Eq. 5), ensuring the EFT remains renormalizable at engineering scales [20].

XI. HARDWARE ARCHITECTURES

The preceding theoretical development culminates in a set of concrete engineering requirements: extreme magnetic gradients ∇B^2, materials capable of sustaining them, and control architectures for flight dynamics. We now specify the hardware that translates the Master Equation into physical technology.

A. The MADA Core

The recursive Magnetic Amplification and Direction Assembly [30, 42] exploits flux frustration in 10–100 μm gaps, creating localized magnetic pressure $P_m = B^2/2\mu_0$ of 203–540 T equivalent in five identical 12-magnet per position MADA arrays [30]. Structural containment requires Ti-6Al-4V or Inconel 718 exoskeletons with ZrO_2 ceramic spacers [30, 36].

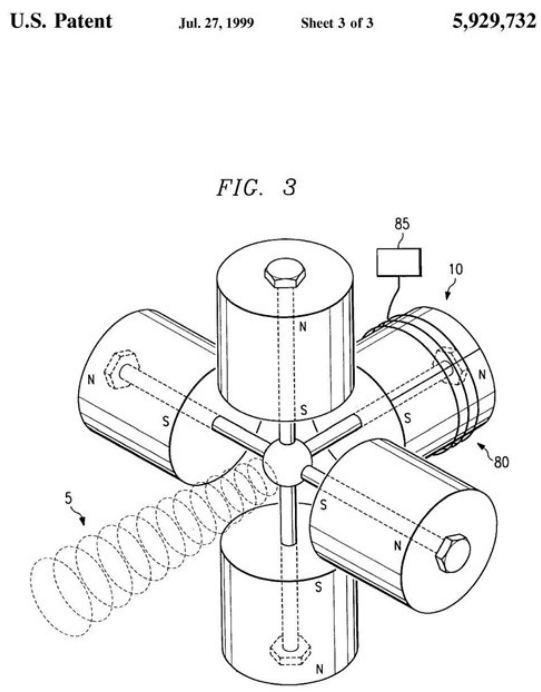

FIG. 6. Original "Lockheed Martin Corporation" magnetic beam amplification apparatus (U.S. Patent 5,929,732 [42]).

B. Hiperco-50 vs. Minnealloy

Minnealloy (α'-$Fe_8(NC)$) represents the theoretical ideal [37, 39]. Its giant saturation magnetization (> 2.9 T) arises from epitaxial strain and interstitial nitrogen occupying octahedral sites in the body-centered tetragonal (bct) lattice, which localizes the 3d electrons and enhances the magnetic moment per iron atom [37, 38]. However, Minnealloy is thermodynamically metastable: at temperatures exceeding 250°C, the nitrogen atoms diffuse

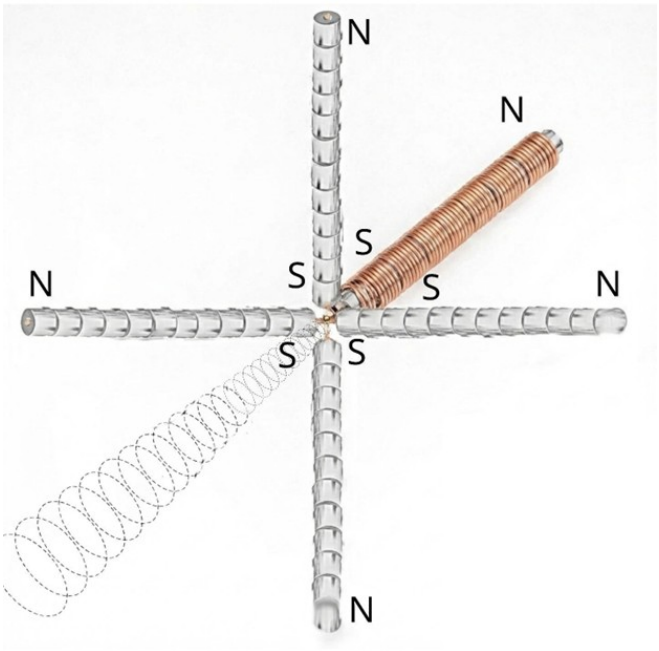

FIG. 7. Single five-position MADA unit showing axially stacked 12-ring-magnet assemblies with south-pole frustration zone at the center, pulsing coil (copper), and helical flux projection (dashed). The opposing like-poles within the 10–100 μm gap force lateral flux compression, generating localized virtual pressures of 203–540 Tesla equivalent in five identical 12-magnet per position MADA arrays [30].

and the compound decomposes into standard α-Fe and γ'-Fe_4N, destroying its giant moment [39]. Consequently, it is reserved exclusively for the passive, thermally benign Scalar-Hydraulic Drive.

Hiperco-50 (Fe-49Co-2V) is the commercial baseline [36]. While offering a lower saturation limit of 2.40 T, its Curie temperature of 940°C makes it exceptionally robust against the immense I^2R heating of active pulsed architectures. The core is constructed using 0.15 mm to 0.35 mm laminations; the 0.15 mm stacks are utilized for high-frequency Burst Mode vectoring, where the skin depth δ at microsecond pulse frequencies ($f \sim 10^6$ Hz) approaches 100 μm [30]. Laminations thicker than 2δ act as shorted turns, shielding the interior from flux and destroying the gradient; therefore the thin stacks ensure full flux penetration and the creation of millions of parallel micro-singularities for millisecond-scale vectoring [30].

The 0.35 mm stacks are reserved for the heavy static lift of the primary core to maximize the iron stacking factor [28]. Because the ordered Fe-Co B2 superlattice phase is brittle, Wire EDM cutting is required, followed by an ordering anneal at 871°C in dry hydrogen [36].

TABLE IV. MADA core alloy specifications [30, 37–39].

Material	Composition	B_s	Thermal Limit	Application
Hiperco-50	Fe-49Co-2V	2.40 T	$> 800^\circ$C	Active ADPG
Minnealloy	α'-$Fe_8(NC)$	∼2.9–3.1 T	$< 250^\circ$C	Passive SHD

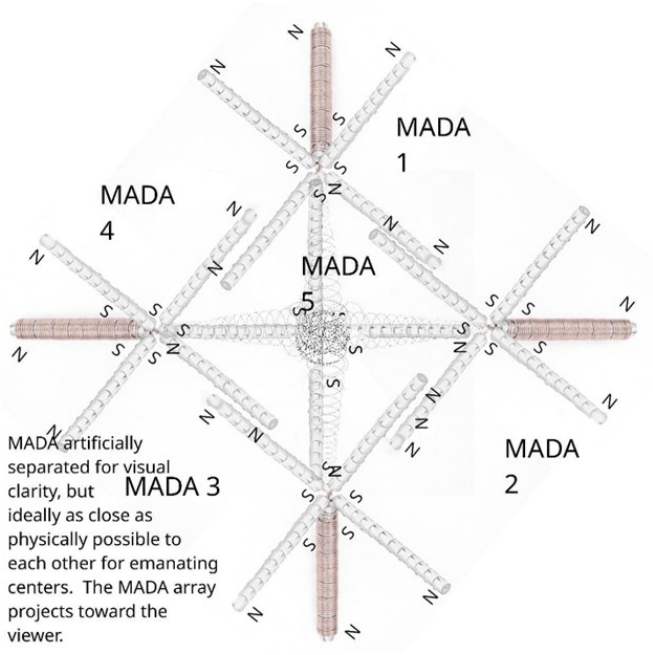

FIG. 8. Five-MADA distributed array configuration (units separated for visual clarity). Each 60-magnet MADA replaces a single magnet in the original Bushman patent geometry [42]: one unopposed MADA on the beam axis (X) and two opposing pairs on the Y and Z axes, all south poles converging at a common center to form the frustrated focusing zone. All three axes are mutually perpendicular; oblique angles are an artifact of the isometric projection [29].

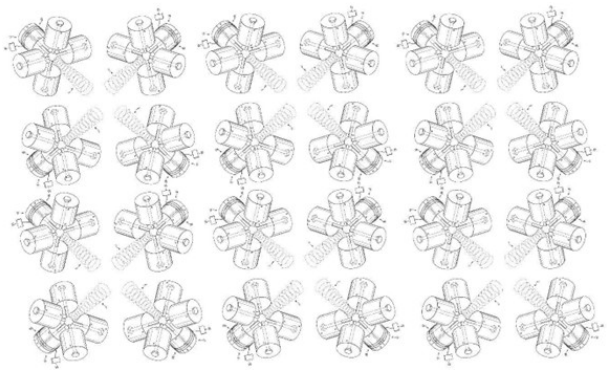

FIG. 9. Recursive tiling of Bushman-type units illustrating the compound geometric gain of the MADA architecture. Each group of four visible MADAs forms the Y- and Z-axis opposing pairs; the fifth (unpictured) sits on the beam axis behind each group, projecting toward the viewer. All south poles converge at a common geometric center to form the frustrated focusing zone [29].

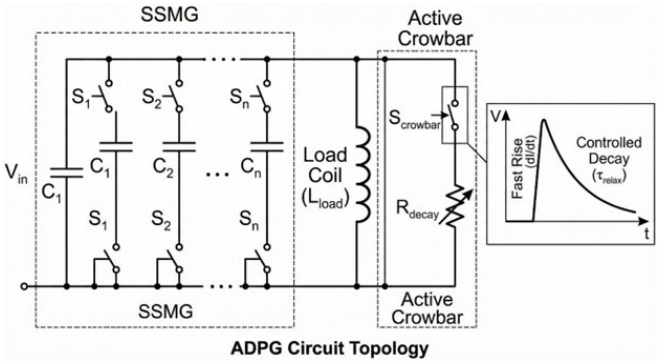

FIG. 10. Schematic of the Asymmetric Dilaton Pump Generator (ADPG). The Solid-State Marx Generator (SSMG) creates the critical nanosecond rise time (dI/dt) required to shock the vacuum metric out of equilibrium. The Active Crowbar modulates the decay phase, dynamically tuning the pulse duration to match the Metric Stiffness Recovery Rate τ_{relax} (Eq. 27) [30].

C. System I: ADPG

The Asymmetric Dilaton Pump Generator operates via temporal asymmetry (dI/dt), driven by a 10-stage Solid-State Marx Generator using SiC MOSFETs (< 20 ns rise time, 10–50 kV pulses) [30]. This "shock" breaks thermodynamic time-reversal symmetry, driving the vacuum into non-equilibrium. The decay phase is managed by an Active Crowbar topology, dynamically tuning the resistance to match τ_{relax} [30]. The Hiperco-50 MADA core is immersed in Solvay Galden PFPE for phase-change cooling [30].

D. System II: Scalar-Hydraulic Drive

The Scalar-Hydraulic Drive, like the ADPG, utilizes partially hybridized cores composed of Minnealloy (α'-$Fe_8(NC)$) or other suitable magnetic circuit materials in conjunction with high-grade permanent magnets—such as neodymium or α''-$Fe_{16}N_2$ (once the latter attains greater commercial availability)—to achieve continuous ∇B^2 generation, completely eliminating the gigawatt-class active power requirements that previously stalled metric propulsion development [29]. Flight control is achieved via Variable Flux Shunting—using Mu-metal mechanical irises to bleed or seal the pressurized magnetic flux—and Distributed Mechanical Gimballing for rapid pitch, yaw, and

roll [29].

The negative gradient in the vacuum force density (Eq. 23) ensures that the net force pushes the physical system away from regions of highest magnetic energy density, creating "Vacuum Buoyancy"—the passive, continuous analog of aerodynamic lift generated by pressure differentials [29, 31]. The Metric Envelope shields the hull from aerodynamic heating at velocities exceeding Mach 26: because the vehicle is stationary with respect to its local metric bubble, atmospheric particles are refractively bent around the hull, completely mitigating plasma sheath formation [28, 29].

To execute highly tactical maneuvers, the drive engages Vacuum Liquefaction at $\omega_{\text{liq}} \approx 50$–$100$ Hz (Eq. 28), transitioning the local metric from an elastic solid-like state to a thixotropic fluid-like state and eliminating the vacuum friction that would otherwise tear the metric bubble during sudden Burst Mode vector changes [29, 32].

For deep-space operations, the flight computer engages Cruise Entrainment. Because the scalar coupling strength λ_H varies by 3–5% over gigaparsec distances due to the running of the vacuum [23, 24], hull-mounted interferometers sense the local background refractive index, and the flight computer applies a micro-radian bias:

$$\theta \approx 4.5\ \mu\text{rad}, \tag{29}$$

to the gimbal angle, ensuring the internal metric gradient matches the recession velocity of the background metric for near-zero-power cruise [29].

XII. CONCLUSION

> *The idea is amusing and enticing; but whether the Almighty is laughing at it and is leading me up the garden path—that I cannot know.*
>
> —Albert Einstein, letter to Conrad Habicht (1905) [48]

The mathematical rectification of the GU-RVG framework stabilizes its theoretical architecture. The chimeric bundle has been mapped to boundary entanglement entropy via the RT functional (Eq. 1), the Zorro construction identified as the HKLL kernel generator (Eq. 3), and the $U(64, 64)$ anomaly cancellation demonstrated via the Atiyah-Singer index theorem with a 14D Green-Schwarz mechanism (Eq. 5). The Swimmer equation's form-degree mismatch is resolved by normal-bundle fiber integration (Eq. 6).

The 95.4 GeV dilaton is characterized with explicit partial widths (Eqs. 13–14) and a combined 3.1σ significance across CMS and ATLAS (Table II), distinguishing it from S2HDM and NMSSM alternatives via its universally trace-anomaly-scaled couplings. The Koide deviation is derived as the 1-loop consequence of the dilaton VEV with $f_\phi \approx 27.2$ TeV (Eq. 10), verified against the explicit PDG computation (Table I). All engineering parameters—$\Theta_{95} \approx 1.54 \times 10^{-11}$, $B_{\text{crit}} \approx 1.53 \times 10^{20}$ T, κ_1, and ζ_{local}—are explicitly defined.

The 19-order-of-magnitude discrepancy between B_{crit} and the extrapolated from QED VMB $B_{\text{opposing}} \approx 20$–$90^+$ T (mass dependent) liftoff threshold is resolved by the Topologically Induced Phase Transition: magnetic helicity generated by MADA flux frustration (Eq. 22) couples to bulk Chern-Simons terms, triggering spontaneous dilaton condensation into a macroscopic N^2-scaling holographic superconductor at the phenomenological phase boundary. The Master Equation of Levitation is derived from Helmholtz first principles (Eq. 25), establishing the phenomenon of Vacuum Buoyancy as the passive propulsive mechanism. The Metric Stiffness Recovery Rate τ_{relax} is obtained from RVM linearization (Eq. 27), grounding the operational states of Vacuum Liquefaction, Burst Mode vectoring, and Cruise Entrainment (Eq. 29) in quantifiable physics.

The WW theorem is evaded via SLSB, thermodynamic consistency is ensured by the $(L_{\text{extra}}/l_p)^{10}$ entropy capacity of the bulk, and the metallurgical constraints of Minnealloy and Hiperco-50 (Table IV) are specified alongside the distinct operational envelopes of the ADPG and Scalar-Hydraulic Drive (Table V). The principal derived quantities are collected in Table VI for the convenience of the reader.

TABLE V. Comparison of the two primary GU-RVG propulsion architectures [29, 30].

Feature	**ADPG**	**Scalar-Hydraulic Drive**
Classification	Active (Electromagnetic)	Passive (Permanent Magnet)
Primary Asymmetry	Temporal: dI/dt	Spatial: ∇B^2
GU Analog	Pumping Swimmer (Dynamic Soliton)	Glider (Static Warp Field)
Control Method	Electronic: Active Crowbar	Mechanical: Variable Flux Shunting
Power Source	External HV Supply	Internal (Geometric Resonance)
Thermodynamics	Open System (High Entropy Exhaust)	Closed/Resonant System (Vacuum Buoyancy)

TABLE VI. Summary of principal derived quantities in the GU-RVG framework.

Quantity	**Symbol**	**Value / Equation**
Dilaton mass	m_ϕ	95.4 GeV
Dilaton decay constant	f_ϕ	≈ 27.2 TeV (Eq. 11)
Vacuum coupling	Θ_{95}	$\approx 1.54 \times 10^{-11}$ (Eq. 20)
Critical field	B_{crit}	$\approx 1.53 \times 10^{20}$ T (Eq. 21)
Phase boundary	B_{opposing}	$B_{\text{opposing}} \approx 20$–$90^+$ T (mass dependent) (Sec. VIII)
Koide deviation	ΔQ	6.17×10^{-6} (Eq. 10)
$\phi \to \gamma\gamma$ width	$\Gamma_{\gamma\gamma}$	$\approx 7.88 \times 10^{-12}$ GeV (Eq. 13)
$\phi \to b\bar{b}$ width	$\Gamma_{b\bar{b}}$	$\approx 2.65 \times 10^{-7}$ GeV (Eq. 14)
$\phi \to \tau\tau$ width	$\Gamma_{\tau\tau}$	$\approx 1.62 \times 10^{-8}$ GeV (Eq. 14)
Diphoton signal strength	$\mu_{\gamma\gamma}$	≈ 0.24 (Table II)
Relaxation frequency	ω_{liq}	50–100 Hz (Eq. 28)
Cruise gimbal bias	θ	≈ 4.5 μrad (Eq. 29)
Gauge group	H	$U(64, 64)$ (Eq. 4)
Bulk entropy capacity	S_{bulk}	$\sim (L_{\text{extra}}/l_p)^{10}$

ACKNOWLEDGMENTS

The active author gratefully acknowledges Eric R. Weinstein for the creation of the Geometric Unity framework, which provides the geometric foundation that is half of the GU-RVG synthesis. The author also acknowledges the experimental teams of the CMS and ATLAS collaborations at CERN, the Belle II collaboration at KEK, and the Particle Data Group, without whose precision measurements none of the phenomenological results presented here would be possible. The work of Joan Solà Peracaula and collaborators on the Running Vacuum Model has been essential to establishing the cosmological boundary conditions for metric engineering.

DATA AVAILABILITY STATEMENT

Empirical lepton masses are from PDG/CODATA 2024 [43, 44]. The 95.4 GeV resonance data are from CMS and ATLAS [6, 7]. Magnetic material specifications derive from Refs. [36, 37, 39].

[1] Y. Koide, "Fermion-Boson Two Body Model of Quarks and Leptons and Cabibbo Mixing," Lett. Nuovo Cimento **34**, 201–205 (1982). DOI: 10.1007/BF02817096.

[2] C. A. Brannen, "The Lepton Masses," Brannen Works, May 2, 2006. Available: `https://www.brannenworks.com/MASSES2.pdf` (viXra:0604.0133).

[3] Y. Sumino, "Family gauge symmetry as an origin of Koide's mass formula and charged lepton spectrum," J. High Energy Phys. **05**, 075 (2009). arXiv:0812.2103 [hep-ph]. DOI: 10.1088/1126-6708/2009/05/075.

[4] J. Kocik, "The Koide Lepton Mass Formula and Geometry of Circles," arXiv:1201.2067 [physics.gen-ph] (2012). DOI: 10.48550/arXiv.1201.2067.

[5] C. McKoy, "The Cogito of Fermion Masses: Two Independent Mathematical Framings of the Koide Formula, a New Geometric Interpretation, and Its Identification with the AdS/CFT Correspondence," Zenodo (2026). DOI: 10.5281/zenodo.19271888.

[6] T. Biekötter, S. Heinemeyer, and G. Weiglein, "The 95.4 GeV di-photon excess at ATLAS and CMS," Phys. Rev. D **109**, 035005 (2024). DOI: 10.1103/PhysRevD.109.035005.

[7] T. Biekötter, S. Heinemeyer, and G. Weiglein, "Mounting evidence for a 95 GeV Higgs boson," J. High Energy Phys. **08**, 201 (2022). DOI: 10.1007/JHEP08(2022)201.

[8] T. Mondal, S. Moretti, and P. Sanyal, "On the CP Nature of the '95 GeV' Anomalies," arXiv:2412.00474 [hep-ph] (2024).

[9] T. Biekötter, S. Heinemeyer, and G. Weiglein, "The CMS di-photon excess at 95 GeV in view of the LHC Run 2 results," Phys. Lett. B **846**, 138217 (2023). DOI: 10.1016/j.physletb.2023.138217.

[10] T. Biekötter *et al.*, "95 GeV Higgs boson and nano-Hertz gravitational waves from domain walls in the N2HDM," arXiv:2505.03592 [hep-ph] (2025).

[11] CMS Collaboration, "Search for a standard model-like Higgs boson in the mass range between 70 and 110 GeV in the diphoton final state in proton-proton collisions at $\sqrt{s} = 13$ TeV," Phys. Lett. B **860**, 139067 (2025). DOI: 10.1016/j.physletb.2024.139067.

[12] J. Lian and J. Cao, "Scalar Resonances near 650 and 95 GeV in the GNMSSM with Correct Dark Matter Relic Abundance," arXiv:2511.04968 [hep-ph] (2025). DOI: 10.48550/arXiv.2511.04968.

[13] T. Biekötter *et al.*, "Unified interpretation of 95 GeV di-photon and di-tau excesses in the Georgi-Machacek Model," arXiv:2509.26155 [hep-ph] (2025).

[14] G. 't Hooft, "Dimensional Reduction in Quantum Gravity," in *Salamfestschrift*, ed. A. Ali *et al.* (World Scientific, Singapore, 1994), pp. 284–296, arXiv:gr-qc/9310026; L. Susskind, "The World as a Hologram," J. Math. Phys. **36**, 6377–6396 (1995). DOI: 10.1063/1.531249.

[15] J. Maldacena, "The Large N Limit of Superconformal Field Theories and Supergravity," Adv. Theor. Math. Phys. **2**, 231–252 (1998). DOI: 10.4310/ATMP.1998.v2.n2.a1. arXiv:hep-th/9711200.

[16] S. Ryu and T. Takayanagi, "Holographic Derivation of Entanglement Entropy from AdS/CFT," Phys. Rev. Lett. **96**, 181602 (2006). DOI: 10.1103/PhysRevLett.96.181602. arXiv:hep-th/0603001.

[17] A. Hamilton, D. Kabat, G. Lifschytz, and D. Lowe, "Local bulk operators in AdS/CFT: A boundary operator expansion," Phys. Rev. D **73**, 086003 (2006). DOI: 10.1103/PhysRevD.73.086003. arXiv:hep-th/0506232.

[18] J. W. Moffat and E. J. Thompson, "On the Complexified Spacetime Manifold Mapping of AdS to dS," arXiv:2511.11658 [gr-qc] (2025).

[19] A. Pomarol, O. Pujolàs, and L. Salas, "Light holographic dilatons near critical points," Phys. Rev. D **110**, 126017 (2024). DOI: 10.1103/PhysRevD.110.126017.

[20] M. B. Green and J. H. Schwarz, "Anomaly cancellations in supersymmetric $D = 10$ gauge theory and superstring theory," Phys. Lett. B **149**, 117–122 (1984). DOI: 10.1016/0370-2693(84)91565-X. See also: L. Álvarez-Gaumé and E. Witten, "Gravitational anomalies," Nucl. Phys. B **234**, 269–330 (1984). DOI: 10.1016/0550-3213(84)90066-X.

[21] D. Tong, "Gauge Theory," Ch. 3: Anomalies, DAMTP lecture notes, University of Cambridge (2018). Available: `https://www.damtp.cam.ac.uk/user/tong/gaugetheory.html`.

[22] E. Weinstein, "Geometric Unity: Author's Working Draft, v 1.0," self-published manuscript (2021). Available: `https://geometricunity.nyc3.digitaloceanspaces.com/Geometric_Unity-Draft-April-1st-2021.pdf`.

[23] J. Solà Peracaula, "The cosmological constant problem and running vacuum in the expanding universe," Philos. Trans. R. Soc. A **380**, 20210182 (2022). DOI: 10.1098/rsta.2021.0182.

[24] J. Solà, A. Gómez-Valent, and J. de Cruz Pérez, "Possible signals of vacuum dynamics in the Universe," Mon. Not. R. Astron. Soc. **478**, 4357–4373 (2018). DOI: 10.1093/mnras/sty1253.

[25] C. Moreno-Pulido and J. Solà Peracaula, "Renormalizing the vacuum energy in cosmological spacetime: implications for the cosmological constant problem," Eur. Phys. J. C **82**, 551 (2022). DOI: 10.1140/epjc/s10052-022-10484-w.

[26] J. Solà, A. Gómez-Valent, and J. de Cruz Pérez, "Running vacuum model versus ΛCDM—a Bayesian analysis," Int. J. Mod. Phys. A **37**, 2250025 (2022). DOI: 10.1142/S0217751X22500257.

[27] A. Gómez-Valent and J. Solà Peracaula, "Composite dark energy and the cosmological tensions," arXiv:2412.15124 [astro-ph.CO] (2024).

[28] J. D. Hofseth, "Refractive Vacuum Gravity (RVG) Unified Field: Disformal QED, the 95 GeV Resonance, and the Metric Engineering of Static Levitation," Gen. Sci. J. (2026). DOI: 10.5281/zenodo.18638071.

[29] J. D. Hofseth, "The Unified Field Scalar-Hydraulic Drive: Metric Engineering via the 95.4 GeV Dilaton Resonance and the Running Vacuum Model," Gen. Sci. J. (2026). DOI: 10.5281/zenodo.18652906.

[30] J. D. Hofseth, "Refractive Vacuum Gravity (RVG) Unified Field: Engineering the Vacuum via the Asymmetric Dilaton Pump Generator (ADPG)," Gen. Sci. J. (2026). DOI: 10.5281/zenodo.18653086.

[31] J. D. Hofseth and E. R. Weinstein, "The Geometric-Refractive Unification: A Definitive Synthesis of Geometric Unity and Refractive Vacuum Gravity," Gen. Sci. J. (2026). DOI: 10.5281/zenodo.18688303.

[32] J. D. Hofseth and E. R. Weinstein, "The Geometric-Refractive Unification: A Definitive Synthesis of the Koide Lepton Anomaly, the 95.4 GeV Dilaton Resonance, and Advanced Metric Engineering," Gen. Sci. J. (2026). DOI: 10.5281/zenodo.19297861.

[33] D. Sachdeva and S. Sadhukhan, "Discussing 125 GeV and 95 GeV excess in light radion model," Phys. Rev. D **101**, 055045 (2020). DOI: 10.1103/PhysRevD.101.055045.

[34] M. Novello, V. A. De Lorenci, J. M. Salim, and R. Klippert, "Geometrical aspects of light propagation in nonlinear electrodynamics," Phys. Rev. D **61**, 045001 (2000). DOI: 10.1103/PhysRevD.61.045001.

[35] H. E. Puthoff, "Polarizable-Vacuum (PV) approach to general relativity," Found. Phys. **32**, 927–943 (2002). DOI: 10.1023/A:1016011413407.

[36] W. R. Wieserman, G. E. Schwarze, and J. M. Niedra, "Magnetic and electrical characteristics of cobalt-based alloys for high-temperature, high-frequency aerospace power conversion applications," NASA/TM-2013-217878 (2013). Available: `https://ntrs.nasa.gov/citations/20140002935`.

[37] N. Ji, L. F. Allard, E. Lara-Curzio, and J.-P. Wang, "The effect of strain induced by Ag underlayer on saturation magnetization of partially ordered $Fe_{16}N_2$ thin films," J. Appl. Phys. **115**, 093910 (2014). DOI: 10.1063/1.4867230.

[38] M. Komuro, Y. Kozono, M. Hanazono, and Y. Sugita, "Magnetic structure of $Fe_{16}N_2$ determined by polarized neutron diffraction on thin-film samples," J. Magn. Magn. Mater. **109**, 63–72 (1992). DOI: 10.1016/0304-8853(92)91024-N.

[39] Y. Jiang *et al.*, "Assessment of Minnealloy fabrication via three routes," AIP Advances **15**, 035008 (2025). DOI: 10.1063/5.0248832.

[40] T. Nguyen and T. Polya, "A Response to Geometric Unity," preprint (2021). Available: `https://files.timothynguyen.org/geometric_unity.pdf`.

[41] J. T. Cox, "Geometric Unity III: Quantization, BRST, and Deformation Complex," preprint (2025). Available: `https://www.researchgate.net/publication/396557263`.

[42] B. B. Bushman, "Magnetic Thrust Device," U.S. Patent 5,929,732, assigned to Lockheed Martin Corporation (1999).

[43] S. Navas *et al.* (Particle Data Group), "Review of Particle Physics," Phys. Rev. D **110**, 030001 (2024). DOI: 10.1103/PhysRevD.110.030001.

[44] Belle II Collaboration, "Measurement of the τ-lepton mass with the Belle II experiment," Phys. Rev. D **108**, 032006 (2023). DOI: 10.1103/PhysRevD.108.032006.

[45] A. Pais, *'Subtle is the Lord...': The Science and the Life of Albert Einstein* (Oxford University Press, Oxford,

1982), p. 235.

[46] P. A. M. Dirac, "The Evolution of the Physicist's Picture of Nature," Sci. Am. **208**(5), 45–53 (1963). DOI: 10.1038/scientificamerican0563-45.

[47] I. I. Rabi, as quoted in L. M. Lederman and D. Teresi, *The God Particle* (Houghton Mifflin, Boston, 1993), p. 169.

[48] A. Einstein, letter to Conrad Habicht [ca. September 1905], in *The Collected Papers of Albert Einstein*, Vol. 5, Doc. 28 (Princeton University Press, Princeton, NJ, 1993).

[49] S. A. Hartnoll, C. P. Herzog, and G. T. Horowitz, "Building a Holographic Superconductor," Phys. Rev. Lett. **101**, 031601 (2008). DOI: 10.1103/PhysRevLett.101.031601. arXiv:0803.3295 [hep-th]. See also: S. A. Hartnoll, C. P. Herzog, and G. T. Horowitz, "Holographic Superconductors," J. High Energy Phys. **12**, 015 (2008). DOI: 10.1088/1126-6708/2008/12/015.

[50] H. K. Moffatt, "The degree of knottedness of tangled vortex lines," J. Fluid Mech. **35**, 117–129 (1969). DOI: 10.1017/S0022112069000991.

[51] J. D. Bekenstein, "The Relation between Physical and Gravitational Geometry," Phys. Rev. D **48**, 3641–3647 (1993). DOI: 10.1103/PhysRevD.48.3641.